SI Appendix for the article "**Quantifying the role of mineral bridges on the fracture resistance of nacre-like composites**"

Madeleine Grossman, Florian Bouville, Kunal Masania*, André R Studart*

Complex Materials, Department of Materials, ETH Zürich, 8093 Zürich, Switzerland

Vacuum-Assisted Magnetic Alignment (VAMA) process

In the VAMA process, a rotating magnetic field is used to align magnetized α-alumina microplatelets suspended in a liquid, while vacuum consolidates the aligned material on a filter; akin to a paper making process. This process results in bulk-scale green bodies of highly aligned platelets. Pressure assisted sintering is then used to consolidate the green bodies into nacre-like scaffolds, which can be infiltrated with monomers to generate brick-and-mortar architectures after polymerization. Mineral bridges can be created between the bricks if alumina platelets with a titania coating are used during the VAMA process. Bridges of controllable size are formed upon dewetting of the titania from the alumina surface during sintering. Mineral interconnectivity is controlled by adjusting the processing temperature (1).

Composite fabrication

Titania-coated alumina microplatelets (Xirallic Crystal Silver T-50, Merck GMBH, Germany) were rendered magnetically responsive by electrostatic surface adsorption of superparamagnetic iron oxide nanoparticles (SPIONs), as described by Erb et al (2). Dry magnetized platelets (20 g, 5 vol%) were suspended by vigorous stirring in a 100mL aqueous solution containing 2% poly(vinyl alcohol) (M_W=13-23 kDa, Sigma Aldrich, Germany), 1% poly(acrylic acid) sodium salt (M_W=8 kDa, Polysciences, USA) and one drop of Antifoam 204 (Sigma Aldrich, Germany). This mixture was then transferred to a laboratory vacuum filtration set-up, encircled by four solenoids generating an in-plane rotating magnetic field. A color change, indicating that platelets had aligned and become more reflective, was observed within 30 seconds. The aligned platelets were subsequently consolidated into a disc-shaped compact (46 mm diameter) by pulling vacuum at 100 mbar for 25 minutes. Green bodies were pre-fired in air at 500 °C for 3 hours to remove the organics before transferring to a Spark Plasma Sintering oven (HP D 10, FCT Systeme GmbH, Germany). Samples were sintered in a 50 mm argon-purged graphite die at varying pressures and temperatures. Heating and cooling rates of 100°C/min were used in the sintering process. Isostatic pressure (5-45 MPa, KIP 100E, P.O. Weber, Germany) was used to infiltrate each sintered ceramic scaffold with a commercial epoxy (Sikadur-300, Sika, Switzerland), which was then oven cured at 120 °C for 2 hours. To ensure complete impregnation, pressure was applied for 10 minutes. This resulted in a maximum porosity of only 0.2% in the final infiltrated scaffolds.

Composite characterization

The volume fraction of mineral phase in the nacre-like composites was measured by Archimedes' displacement. Flexural tests were performed on a universal testing machine (Autograph AGS-X, Shimadzu, Japan) on samples cut and polished to 25 mm x 2 mm x 1.5 mm, as specified by ASTM designation C1161 − 13. Single-edge notched bending tests were performed on samples cut and polished to 15 mm x 3 mm x 3 mm. A notch length of 1.5 mm was produced perpendicular to the plane of platelet alignment and sharpened with a razor blade to produce a local radius of curvature of <40 μm, as specified by ASTM designation D5045 – 99 (3). The flexural strength (σ_c), stress intensity factor (K_I and K_{IC}) and work of fracture data were calculated as described in ASTM designation C1421 – 10 (4). Quantification of titania feature size and platelet cluster size was performed by image analysis of scanning electron micrograph (SEM) cross sections. Details of such analysis was previously reported by Grossman *et al* (1). Cross sections for microstructural analysis were flat polished with a broad ion beam mill (IM4000, Hitachi, Japan) and imaged using a (LEO 1530) scanning electron microscope in backscatter mode to differentiate between phases by relative density. Images were processed using the Fiji software packages (5-8). Each high contrast pixel was assigned as belonging to one of four titania feature types: unconnected continuous coatings, mineral bridges, unconnected asperities and thin films within platelet clusters, which were identified by feature size. The proportion of mineral bridges and thin films within clusters with respect to all the titania features was taken as the fraction of mineral bridges, γ. This is a relative quantity that is taken here as a proxy for the fraction of the platelet surface that is connected to adjacent platelets through mineral bridges.

Characterization of interplatelet connectivity

Broad ion beam polished cross-sections were imaged with SEM to confirm that the scaffolds selected for the study have different mineral bridge connectivity between the platelets and to eventually quantify the density of bridges (Fig. 1B). In all of the samples, titania features between 75 and 150 nm were identified as mineral bridges, since these length scales lie within the range of the inter-platelet distance for these 60 vol% mineral composites. Titania feature sizes outside the 75-150 nm range were found to either form (i) unconnected asperities at larger sizes or (ii) thin films within platelet clusters and unconnected continuous coatings at smaller sizes, depending on the sintering temperature. In samples sintered below 900 °C, the majority of smaller features are attributed to unconnected continuous coatings (Fig. 1C). In samples sintered at 900 °C and above, some titania features grow to sizes in excess of 150 nm to generate large unconnected titania asperities (> 150 nm). This results from unconstrained Ostwald ripening of the titania far from neighboring platelets. At smaller length scales (< 75 nm), scaffolds sintered at or above 900 °C show titania features in the form of thin, continuous titania phase formed within clusters of platelets.

The image analysis shows that a large fraction of platelet clusters was observed in scaffolds sintered at the elevated temperatures of 900 and 1000 °C (Fig. 1D and Fig. S1). This clustering effect results from local rearrangement and densification of platelets mediated by the sintering of the fine-grained titania phase at these high temperatures. By contrast, platelets in scaffolds sintered at 700 °C and 800 °C were

found to only interact with their nearest neighbors without forming clusters. The onset of clustering likely occurs in the range 800 °C to 900 °C.

Estimation of fraction of mineral bridges

The fraction of mineral bridges (γ), was calculated with the following equation:

$$\gamma = \frac{\sum mb + \sum tfc}{\sum mb + \sum tfc + \sum ucc + \sum ua} \text{ (Eq. S1)}$$

where: $\sum mb$ is the sum of pixels in mineral bridges,
$\sum tfc$ is the sum of pixels in thin films within clusters,
$\sum ucc$ is the sum of pixels in unconnected continuous coatings,
$\sum ua$ is the sum of pixels in unconnected asperities.

Because the material is transversely isotropic, the areal fraction measured by image analysis is also equal to the volume fraction material in the composite. Thus, γ represents the areal and volume fraction of titania that forms bridges between platelets.

Inter-cluster fracture in composites sintered at 1000°C

Since the scaffolds exhibit constant mineral volume fraction, the formation of locally dense strong clusters requires concurrent formation of weaker regions with lower mineral density. Such weaker regions lead to an interconnected path where the chance for a potential fracture to take place is significantly higher (Fig 1B). Indeed, the cracks in samples sintered at 1000 °C was found to follow a very tortuous path, which likely reflects these weak and less dense paths (Fig. S2). The presence of a percolating network of weak regions might also be the reason for the low elastic modulus obtained for samples sintered at 1000 °C (Fig. 2B). Despite the formation of large clusters already at 900 °C, we experimentally observed that these clusters are still weak enough to be penetrated by propagating cracks. Thus, our results indicate that the fracture mechanism changes from intra-cluster to inter-cluster as the sintering temperature increases from 900 to 1000 °C. This is analogous to the intragranular and intergranular fracture regimes typically observed in polycrystalline ceramics (9).

Composite strength from shear lag model

Using a rule of mixture approach, the shear lag model predicts the composite strength to vary as follows:

$$\sigma_c = \alpha V_p \sigma_p + (1 - V_p)\sigma_m \quad \text{(Eq. S2)(10)}$$

where α is a stress transfer efficiency term, V_p is the volume fraction of platelets, and σ_p and σ_m are the platelet strength and matrix strength, respectively. The stress transfer term α depends on the fracture behavior of the composite. For composites

failing in pullout mode containing square platelets in a plastic matrix (11) the stress transfer efficiency term has been previously derived as

$$\alpha = \frac{\tau S}{2\sigma_p} \quad \text{(Eq. S3)}$$

which results in the simplified relationship:

$$\sigma_c = \frac{\tau S V_p}{2} + (1 - V_p)\sigma_m, \quad \text{(Eq. S4)}$$

where τ is shear strength of the platelet-matrix interface and *S* is the aspect ratio of the platelet.

Estimation of composite strength under platelet fracture mode

Under platelet fracture mode, the strength of the composite is determined by the fracture strength of the platelet. In this case, the stress transfer efficiency term α for square platelets in brick-and-mortar geometries (11) is given by:

$$\alpha = \frac{1}{2} \quad \text{(Eq. S5)}$$

Introducing this term into Eq. 1 shown in the main text leads to the upper limit for the composite strength:

$$\sigma_{c,max} = \frac{1}{2}\sigma_p V_p + \left(1 - V_p\right)\sigma_m \quad \text{(Eq. S6)}$$

Assuming the stresses to be carried predominantly by the stiff platelets (see discussion in the main text), this equation can be simplified to:

$$\sigma_{c,max} \approx \frac{1}{2}\sigma_p V_p \quad \text{(Eq. S7)}$$

Calculation of the platelet residual stress from observed deflection

To verify if the residual stresses introduced in the nacre-like scaffolds during pressing can reach high stress levels in the range 2-4 GPa, we first measured the deflection of an individual platelet that is supported by adjacent particles in a representative specimen. The residual stress expected in the exemplary supported platelet shown in Figure S4 can be estimated using the following equation (12):

$$\lambda = \sigma_{bending} = \frac{MY}{I} \quad \text{(Eq. S8)}$$

where Y is the distance to the centroid (d/2 for the edge of the platelet) and M is the bending moment given by

$$M = F_y \cdot \frac{L}{2} \quad \text{(Eq. S9)}$$

where F_y is the load in y (through the platelet thickness) and L is the supported length.

The load F_y is given by

$$F_y = \frac{48EI\delta_y}{L^3} \quad \text{(Eq. S10)}$$

where *I* is the second moment of area, *E* is the elastic modulus and δ_y is the deflection in y.

The second moment of area *I* is given by

$$I = \frac{bd^3}{12} \quad \text{(Eq. S11)}$$

where *b* and *d* are the width and the thickness of the platelet, respectively.

Introducing Eq. S5-S7 into Eq. S4, leads to:

$$\lambda = \frac{12E\delta_y d}{L^2} \quad \text{(Eq. S12)}$$

From the scanning electron micrograph shown in Figure S4, we can measure the supported length and deflection in y, which results in an estimated residual stress of 6.4 GPa

Calculation of the platelet residual stresses from bending curvature

The range of residual stresses introduced in the platelets can also be calculated from the bending curvature of individual platelets through image analysis of the SEM images. From the bending curvature, we obtain an estimate of the residual stress (λ_x) using the following relation:

$$\lambda_x(\tfrac{e}{2}) = \frac{e}{2} E \frac{1}{\rho(x)} \quad \text{(Eq. S13)}$$

with e being the platelet thickness, E the Young's modulus of the platelets and $\rho(x)$ the radius of curvature (reciprocal of the curvature) at each point, x, along the length of the platelet. Our estimates indicate that the residual stress reaches an average value of 1 GPa for a representative sample hot-pressed at 700 °C and 45 MPa (Fig. S3F). Such stresses can achieve even higher values in the range of 4-6 GPa for the most bent platelet in the population of data.

Supporting Figures and Table

Table S1: Elastic modulus and surface energy of alumina obtained from the literature and average thickness of the platelets used in the study

Elastic Modulus Alumina	400 GPa
Surface Energy Alumina	5.8 J/m^2 [12]
Average Platelet Thickness, Crystal Silver T50 10	210 nm
Average Platelet Thickness, Microsilver T61 10	132 nm

A 900 ˚C, 15 MPa

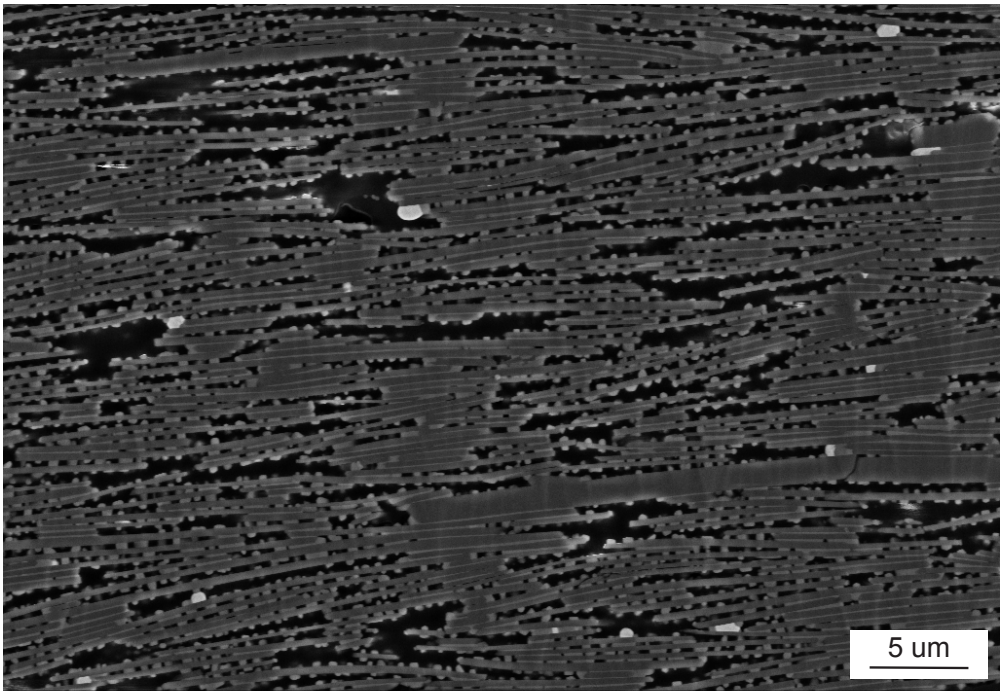

B 1000 ˚C, 5 MPa

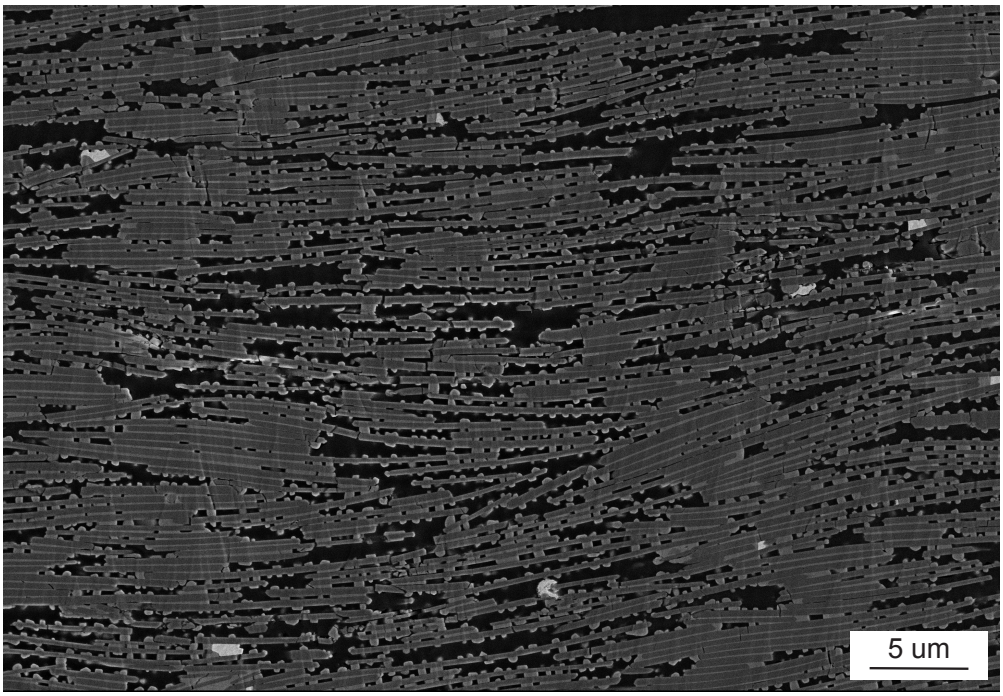

Fig. S1. Cluster formation increases with sintering temperature from 900 ºC to 1000 ºC resulting in larger gaps between clusters at 1000 ºC.

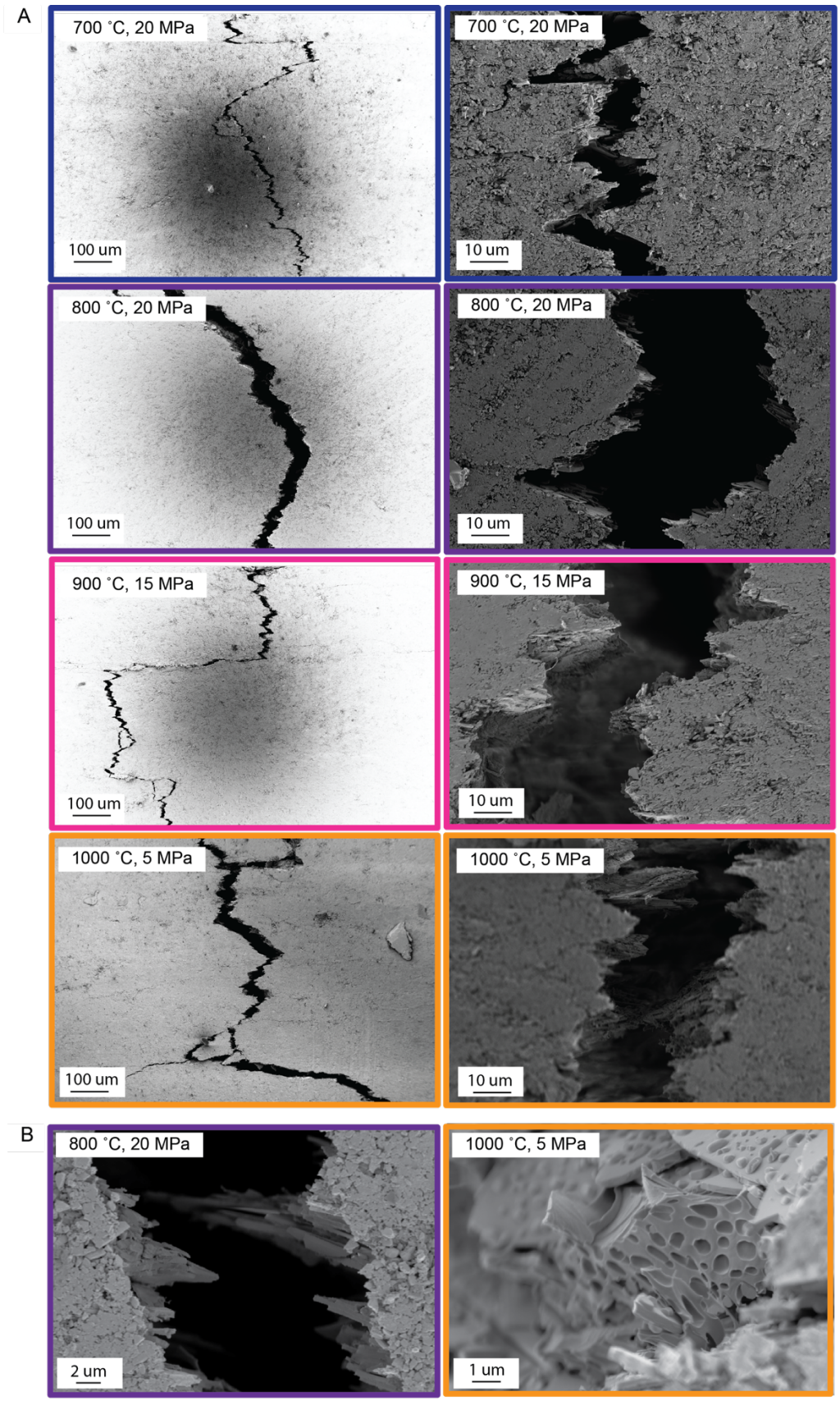

Fig. S2. Shows (A) SEMs of crack propagation paths and interfaces in brick and mortar structures obtained at different temperatures and pressures and (B) zoom in images demonstrating composition dependent, dominant failure mechanisms of pull-out (800 °C) or platelet fracture (1000 °C).

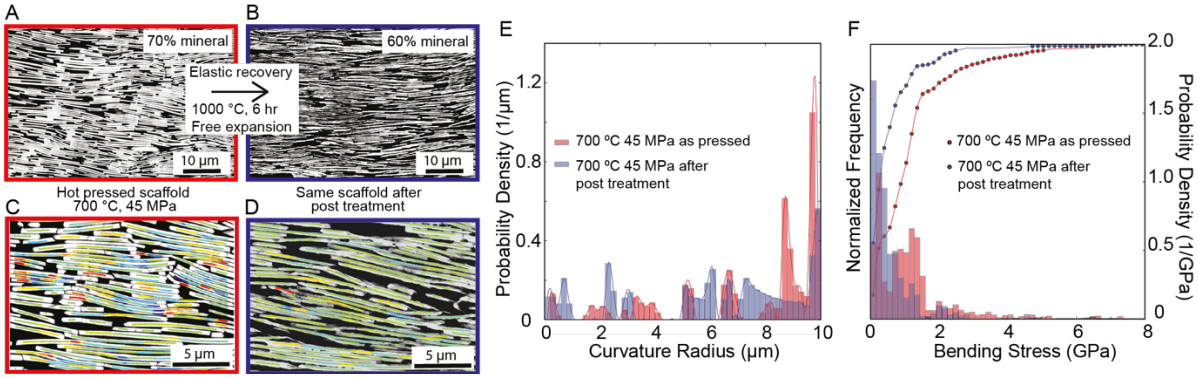

Fig. S3. Bending residual stresses introduced during pressure-assisted sintering of nacre-like scaffolds. (A) SEM image of a representative scaffold, as hot pressed. Platelets appear to be fixed into an elastically stressed, bent configuration after hot-pressing. (B) Heat treatment of the scaffold allows some platelets to elastically recover to their unstressed configuration. Image analysis of scaffold SEM micrographs before (C) and after (D) the heat treatment quantifies the magnitude of curvature in the bent platelets. The color code represents increasing curvature from cold to hot colors. The radius of curvature measured from such images are shown in (E). (F) Cumulative probability density of bending stresses estimated from the measured curvatures (Fig S4).

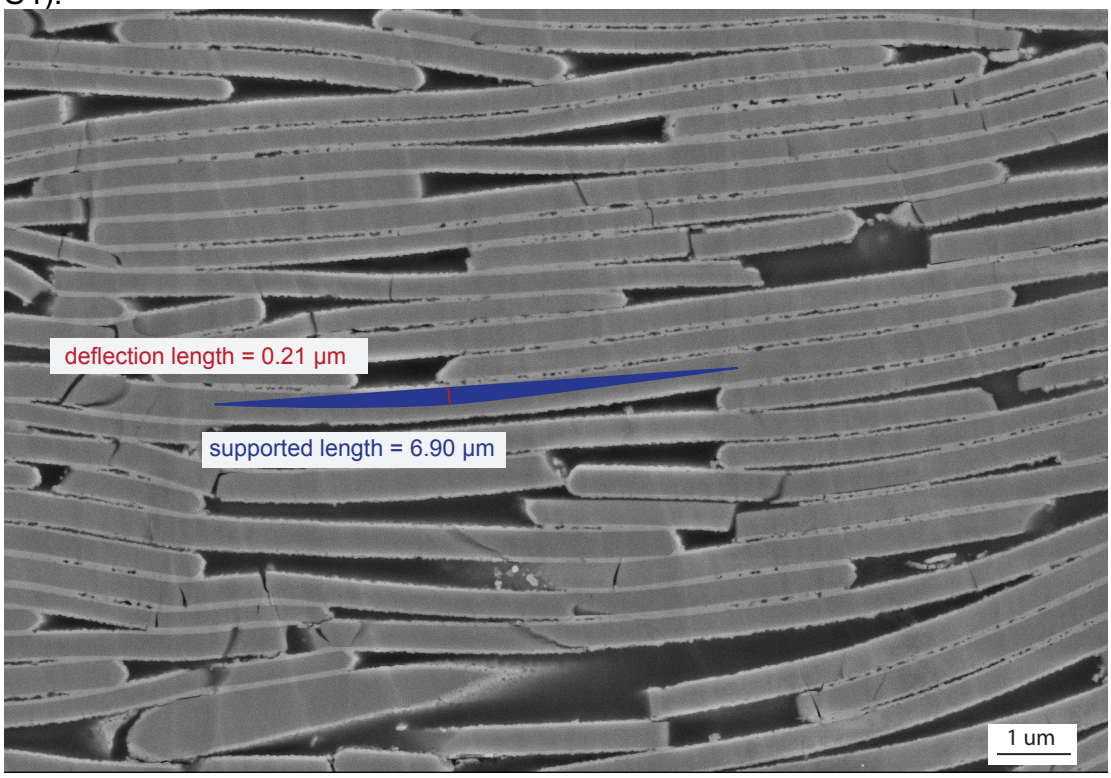

Fig. S4. Significant bending deformations after sintering a sample at 800 °C and 20 MPa. The indicated deflection and supported lengths were used to estimate the residual stresses on the supported platelet.

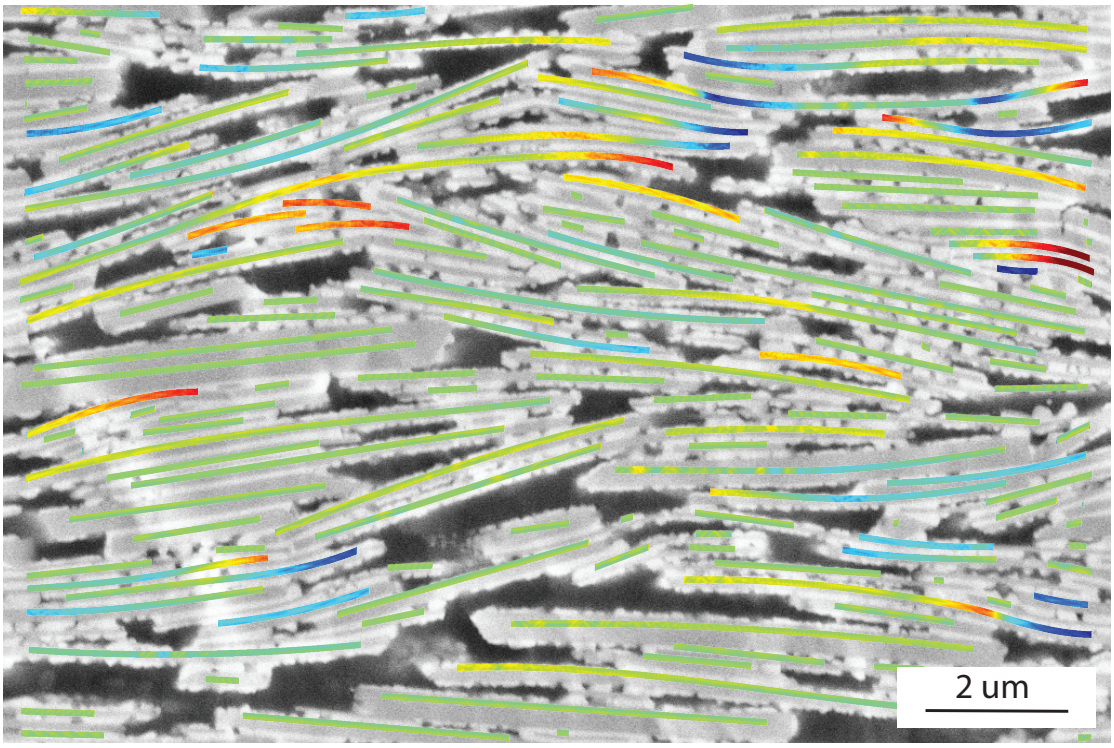

Fig. S5. Smaller grade titania-coated platelets show significant bending deformations after sintering under minimal external pressure (5 MPa)

SI References

1. Grossman M*, et al.* (2017) Mineral Nano-Interconnectivity Stiffens and Toughens Nacre-like Composite Materials. *Advanced Materials* 29(8).
2. Erb RM, Libanori R, Rothfuchs N, & Studart AR (2012) Composites reinforced in three dimensions by using low magnetic fields. *Science* 335(6065):199-204.
3. ASTM-D5045 (1999) Standard Test Method for Plane-Strain Fracture Toughness and Strain-Energy Release Rate of Plastic Materials. in *ASTM* (American Society for Testing and Materials, West Conshohocken).
4. C1421-10 A (2010) Standard Test Methods for Determination of Fracture Toughness of Advanced Ceramics at Ambient Temperature. (American Society for Testing and Materials, West Conshohocken).
5. Schindelin J*, et al.* (2012) Fiji: an open-source platform for biological-image analysis. *Nat Methods* 9(7):676-682.
6. Preibisch S, Saalfeld S, & Tomancak P (2009) Globally optimal stitching of tiled 3D microscopic image acquisitions. *Bioinformatics* 25(11):1463-1465.
7. Hildebrand T & Ruegsegger P (1997) A new method for the model-independent assessment of thickness in three-dimensional images. *J Microsc-Oxford* 185:67-75.
8. Dougherty R & Kunzelmann KH (2007) Computing Local Thickness of 3D Structures with ImageJ. *Microscopy and Microanalysis* 13(Supplement S02):1678-1679.
9. Heuer AH (1969) Transgranular and Intergranular Fracture in Polycrystalline Alumina. *J Am Ceram Soc* 52(9):510.
10. Gao HJ, Ji BH, Jager IL, Arzt E, & Fratzl P (2003) Materials become insensitive to flaws at nanoscale: Lessons from nature. *P Natl Acad Sci USA* 100(10):5597-5600.
11. Glavinchevski, B.; Piggott, M., Steel Disk Reinforced Polycarbonate. *J Mater Sci* **1973,** *8* (10), 1373-1382.
12. Hibbeler, R. C., *Statics and mechanics of materials*. Pearson Higher Ed: **2013**.
13. Wiederhorn SM (1984) Brittle-Fracture and Toughening Mechanisms in Ceramics. *Annu Rev Mater Sci* 14:373-403.